López Boada, B., López Boada, M. J. and Zhang, H. (2019). Sensor fusion based on a Dual Kalman Filter for estimation of road irregularities and vehicle mass under static and dynamic conditions. *IEEE/ASME Transactions on Mechatronics,* 24(3), pp. 1075 - 1086.

DOI: 10.1109/TMECH.2019.2909977

This article has been accepted for publication in a future issue of this journal, but has not been fully edited. Content may change prior to final publication. Citation information: DOI 10.1109/TMECH.2019.2909977, IEEE/ASME Transactions on Mechatronics

Sensor fusion based on a Dual Kalman filter for estimation of road irregularities and vehicle mass under static and dynamic conditions

Beatriz L. Boada, Maria Jesus L. Boada and Hui Zhang

***Abstract*—Mass is an important parameter in vehicle dynamics because it affects not only safety but also comfort. The mass influences the three movements corresponding to vehicle dynamics. Therefore, having an accurate value of mass is essential for having a suitable model which will lead to proper controller and observer operation. Additionally, unlike other vehicle parameters, the mass can vary during a trip due to loading and unloading items and passengers onto the vehicle, greatly influencing its dynamics. This is critical in heavy vehicles where the mass can vary by around 400%. Therefore, the mass must be updated on-line. The novelty of this paper is the construction of a state-parameter observer which allows the mass under static and dynamic driving conditions to be estimated using measurements from sensors that can be mounted easily on vehicles. In this study, a vertical complete model is considered based on the dual Kalman filter for mass and road irregularities estimation using the data obtained from suspension deflection sensors and a vertical accelerometer. Both simulation and experimental results are carried out to prove the effectiveness of the proposed algorithm.**

***Index Terms*—Vehicle mass estimation; road profile estimation; multisensor systems; dual Kalman Filter.**

I. Introduction

TODAY there is a good deal of research focused on designing vehicle safety systems such as ABS (Anti-lock Brake System), ESP (Electronic Stability Program), RSC (Roll Stability Control) and active suspension systems, to be installed on vehicles to improve their behavior in terms of stability, handling and comfort [1]-[5]. These controllers need detailed information about vehicle dynamics through different variables. Some of these cannot be measured directly by sensors or their cost is so high that mounting them on production vehicles is not viable. For this reason, these variables must be estimated using observers [6]-[11]. The majority of research related to the design of controllers and observers uses mathematical models which need a detailed information about their parameters. In regards to parameters, in most cases they are assumed to be known and time invariant. However, this is not always true because some of them may vary considerably during the vehicle's life cycle or while driving. In this case, it is necessary to continuously obtain information about the parameters from direct sensor measurements or indirect measurements (estimations).

One of the vehicle parameters that has received most attention for its estimation is vehicle mass. Mass is a critical parameter concerning vehicle dynamics because it affects not only safety but also comfort. The mass influences the three movements corresponding to vehicle dynamics: longitudinal, lateral and vertical. Therefore, an accurate value of mass is essential for having a suitable model which will lead to proper controller and observer operation[12]-[14]. Additionally, unlike other vehicle parameters, the mass can vary during a trip due to the loading and unloading items and passengers onto the vehicle, greatly influencing hugely onto its dynamics. This is critical in heavy vehicles where the mass can vary by around 400% [15]. Therefore, the mass must be updated online.

In the literature, some research on mass estimation can be found. Wenzel et al. [16] use a DEKF (Dual Extended Kalman Filter) to estimate simultaneously both states and parameters using a four-wheel vehicle model with different interchangeable tire models. The parameters to be estimated are mass, moment of inertia and position of the COG (Centre of Gravity). Results, taking into account combined braking and cornering, as well as measurement noise, show the efficacy of the estimator with errors in mass estimation less than 4%. Nevertheless, results are obtained at low speed and show a great dependence on the tire model used. Fathy et al. [17] propose an algorithm based on the idea that inertial dynamics have a greater influence on vehicle motion during certain types of maneuvers. In this case, when these maneuvers are detected by a *fuzzy supervisor*, the mass is estimated using a RLS (Recursive Least Squares) method. Both simulations and experimental results demonstrate the viability of the proposed approach. A drawback of this method is that the speed of convergence depends on the persistence of driving conditions in which the motion is considered as "significant and predominantly longitudinal". Maalej et al. [18] propose an event-based electric vehicle mass and grade estimation using a longitudinal model and RLS method with variable forgetting factors. The main advantage of this approach is that it does not require torque measurements from the propulsion system, and therefore, it can be used for different types of vehicles. Experimental results show the efficacy of the proposed ap-

Corresponding author: Beatriz L. Boada is with the Department of Mechanical Engineering, Research Group MECATRAN, Research Institute of Vehicle Safety (ISVA), University of Carlos III de Madrid, Leganes, Madrid, Spain. Phone: (+34) 916249168, Fax: (+34) 916249420, e-mail: bboada@ing.uc3m.es

M.J.L. Boada is with the Department of Mechanical Engineering, Research Group MECATRAN, Research Institute of Vehicle Safety (ISVA), University of Carlos III de Madrid, Leganes, Madrid, Spain. e-mail: mjboada@ing.uc3m.es

H. Zhang is with the Department of Automotive Engineering, School of Transportation Science and Engineering, Beihang University, Beijing, China. e-mail: huizhang285@gmail.com

Manuscript received April 19, 2005; revised August 26, 2015.

This article has been accepted for publication in a future issue of this journal, but has not been fully edited. Content may change prior to final publication. Citation information: DOI 10.1109/TMECH.2019.2909977, IEEE/ASME Transactions on Mechatronics

proach obtaining an error less than 3% even with noisy power measurements. Nevertheless, these results are obtained taking into account a flat road and a maximum vehicle speed of 40 km/h. In [19], a four-wheel vehicle model and a DUKF (Dual Unscented Kalman filter) are used to simultaneously identify inertial parameters and states. As in [17], the mass estimation algorithm is only activated when the vehicle is moving and under certain driving situations. Although, both simulation and experimental results show the viability of this approach, it is assumed that the tire-road friction coefficient is known, which is not true in real situations. Jordan et al. [20] use KF (Kalman filter) with a simplified 1/4-vehicle model for mass estimation. Additionally, a longitudinal vehicle model is combined with the previous one in order to obtain the mass distribution. The main advantage of this method is that it is based on measurements obtained from sensors that are available for modern vehicles. Nevertheless, the major drawback is that the model does not take into account the pitch and roll movements so that it does not show good results for rapid longitudinal and lateral accelerations.

Two key aspects to be taken into account in vehicle parameter estimation are the model and analytical method used. The most common methods are RLS, Gradient and KF [21]-[24]. In [25], a comparison between these methods to estimate inertial parameters has been carried out. Conclusions obtained from this study show that RLS and KF have the advantages of simplicity and fast convergence, but they cannot be used with nonlinear systems. On the other hand, the Gradient method can be used with nonlinear systems while it has the disadvantage of being sensitive to the gradient gain. Finally, the extended KF and unscented KF methods show better performance in comparison with the previous ones.

As regards vehicle models, most of them consider the longitudinal and lateral vehicle dynamics [26]-[27]. The major problem in using these models, mainly in parameters estimation, is that the vehicle is required to be moving. As previously indicated, this increases the time of convergence. To solve this problem, vehicle vertical dynamic models, which take into account the vertical suspension deflections, can be used. Suspension deflection can be directly measured through a potentiometer or an LVDT (Linear Variable Differential Transformer) which are both relatively economical and practical to mount. Nowadays, vehicles equipped with active suspension incorporate these kinds of sensors. Additionally, their cost continues to decrease. One of the issues involved in using vehicle vertical models for estimation is that the irregularities of the road have an important influence on the results obtained, so that it is necessary to have continuous information about them through direct measurements (that represent, in most cases, a costly solution) or through estimation.

Taking into consideration all of the previous ideas, the main contribution of this paper is the estimation of the vehicle mass under static and dynamic driving conditions using measurements from sensors which are installed on almost all production vehicles as a standard equipment such as accelerometers. They are also being used more and more in the design of active/semiactive suspension systems such as suspension deflection sensors. As previously mentioned, these sensors are relatively economical and practical to mount. A complete vertical model is considered because it allows the mass to be estimated continuously, independent of driving conditions or whether the vehicle is moving or not, reducing the time of convergence. This model takes into account the pitch and roll movements of the vehicle so that the effectivity of the mass estimation is increased. Additionally, to solve the problem regarding the lack of knowledge of road irregularities, a Dual Kalman filter (DKF) is used. DKF combines two separated Kalman filters. One of them estimates the vehicle states (road irregularities, among others) whereas the other one estimates the vehicle mass. One of the advantages of DKF is that it is possible to disconnect the mass estimator once the mass estimation converges to a certain value.

The outline of the paper is as follows. Section II describes the structure of observer designed based on DKF. Section III gives a description of the vehicle model in this study. In this paper, a complete suspension vehicle model is considered in order to estimate its mass and the road roughness. The state space system based on the vehicle model described in Section III is presented in Section IV. In Section V, a DKF is designed for estimation of the mass and the road roughness. The DKF uses data obtained from sensors which are easily mounted on vehicles such as deflection suspension and angular rate sensors. Both simulation and experimental results are shown in Section VI as is a discussion to prove the effectiveness of the proposed algorithm. Finally, Section VII summarizes, concludes and proposes some future work.

II. State/parameter estimator structure

The proposed state/parameter estimator structure is shown in Figure 1. To deal with the problem of estimating the vehicle mass on-line, a DKF is considered using a complete suspension full car (see Section III). The use of a suspension model allows mass to be estimated not only under dynamic driving conditions but also under static ones. Additionally, this model enables estimation of the road irregularities. This is very useful due to the fact that they greatly influence vehicle dynamics in terms of passenger comfort and road safety. Accordingly, the DKF designed is formed by two Kalman filters: the state Kalman filter and the parameter Kalman. The former estimates the road irregularities and the latter estimates the mass.

The DKF combines measurements from different sensors to estimate states and parameters. This study uses four suspension deflection sensors, which are mounted in each vehicle suspension, and an accelerometer, which is mounted at the center of gravity of vehicle [28]. These sensors can be easily mounted on the vehicle and are not expensive. Some inputs for DKF need to be calculated from data obtained directly from these sensors. This is the case of the vertical displacement of the vehicle Center of Gravity (COG). This value is obtained by a double trapezoidal numerical integration of vertical acceleration.

A high-pass filter with a cutoff frequency of 5 Hz is used to eliminate the drift data due to the amplification of measurements errors when the acceleration is integrated, and

This article has been accepted for publication in a future issue of this journal, but has not been fully edited. Content may change prior to final publication. Citation information: DOI 10.1109/TMECH.2019.2909977, IEEE/ASME Transactions on Mechatronics

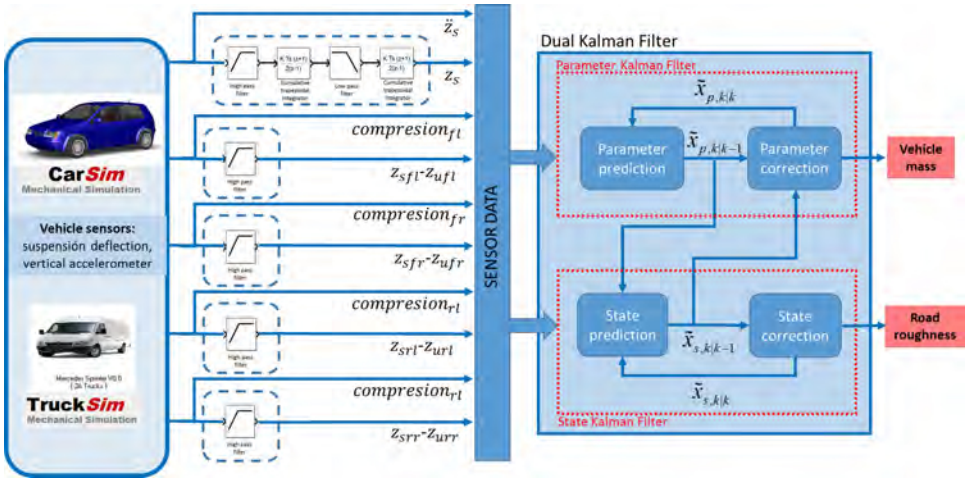

Fig. 1: DKF-based state/parameter estimator structure

a low-pass filter with a cutoff frequency of 15 Hz is used to eliminate the noise of this signal due to the fast up and downward vehicle body movement. These cutoff frequencies have been selected taking into account [29]. Additionally, it was necessary to eliminate the drift data of the suspension deflection sensor measurements using a high-pass filter with a cutoff frequency of 15 Hz. This value has been chosen after performing a frequential analysis.

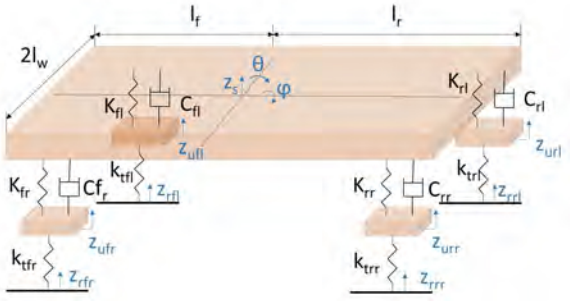

Fig. 2: 7-DOF vehicle model with suspension system

III. Fundamentals of Vehicle Modeling

The vehicle model used for the estimation process of vehicle mass and road irregularities is a suspension full car model as shown in Figure 2. This model is a 7-DOF (Degree of Freedom) model which is described by the following equations:

- Roll motion of sprung mass:

$$\begin{aligned} I_x\ddot{\varphi} =& -C_{fl}l_w(\dot{z}_{sfl}-\dot{z}_{ufl})+C_{fr}l_w(\dot{z}_{sfr}-\dot{z}_{ufr}) \\ & -C_{rl}l_w(\dot{z}_{srl}-\dot{z}_{url})+C_{rr}l_w(\dot{z}_{srr}-\dot{z}_{urr}) \\ & -K_{fl}l_w(z_{sfl}-z_{ufl})+K_{fr}l_w(z_{sfr}-z_{ufr}) \\ & -K_{rl}l_w(z_{srl}-z_{url})+K_{rr}l_w(z_{srr}-z_{urr}) \end{aligned} \tag{1}$$

- Pitch motion of sprung mass:

$$\begin{aligned} I_y\ddot{\theta} =& -C_{fl}l_f(\dot{z}_{sfl}-\dot{z}_{ufl})-C_{fr}l_f(\dot{z}_{sfr}-\dot{z}_{ufr}) \\ & +C_{rl}l_r(\dot{z}_{srl}-\dot{z}_{url})+C_{rr}l_r(\dot{z}_{srr}-\dot{z}_{urr}) \\ & -K_{fl}l_f(z_{sfl}-z_{ufl})-K_{fr}l_f(z_{sfr}-z_{ufr}) \\ & +K_{rl}l_r(z_{srl}-z_{url})+K_{rr}l_r(z_{srr}-z_{urr}) \end{aligned} \tag{2}$$

- Bounce motion of sprung mass:

$$\begin{aligned} m_s\ddot{z}_s =& -C_{fl}(\dot{z}_{sfl}-\dot{z}_{ufl})-C_{fr}(\dot{z}_{sfr}-\dot{z}_{ufr}) \\ & -C_{rl}(\dot{z}_{srl}-\dot{z}_{url})-C_{rr}(\dot{z}_{srr}-\dot{z}_{urr}) \\ & -K_{fl}(z_{sfl}-z_{ufl})-K_{fr}(z_{sfr}-z_{ufr}) \\ & -K_{rl}(z_{srl}-z_{url})-K_{rr}(z_{srr}-z_{urr}) \end{aligned} \tag{3}$$

- Vertical wheel motion:

$$\begin{aligned} m_{ufl}\ddot{z}_{ufl} &= C_{fl}(\dot{z}_{sfl}-\dot{z}_{ufl})+K_{fl}(z_{sfl}-z_{ufl}) \\ & \quad -K_{tf}z_{ufl}+K_{tf}z_{rfl} \\ m_{ufr}\ddot{z}_{ufr} &= C_{fr}(\dot{z}_{sfr}-\dot{z}_{ufr})+K_{fr}(z_{sfr}-z_{ufr}) \\ & \quad -K_{tf}z_{ufr}+K_{tf}z_{rfr} \\ m_{url}\ddot{z}_{url} &= C_{rl}(\dot{z}_{srl}-\dot{z}_{url})+K_{rl}(z_{srl}-z_{url}) \\ & \quad -K_{tr}z_{url}+K_{tr}z_{rrl} \\ m_{urr}\ddot{z}_{urr} &= C_{rr}(\dot{z}_{srr}-\dot{z}_{urr})+K_{rr}(z_{srr}-z_{urr}) \\ & \quad -K_{tr}z_{urr}+K_{tr}z_{rrr} \end{aligned} \tag{4}$$

where

$$\begin{aligned} z_{sfl} &= z_s+l_w\varphi+l_f\theta;\ \ z_{sfr}=z_s-l_w\varphi+l_f\theta \\ z_{srl} &= z_s+l_w\varphi-l_r\theta;\ \ z_{srr}=z_s-l_w\varphi-l_r\theta \end{aligned} \tag{5}$$

and the subscripts fl, fr, rl and rr indicate front left, front right, rear left and rear right, respectively. In Table I a description of parameters is given.

TABLE I: Parameters for complete suspension vehicle model

Parameter	Description	Unit
θ	Pitch angle	rad
φ	Roll angle	rad
$C_i\ (i=fl,fr,rl,rr)$	Damping of car body	N/m
I_x	Roll inertia moment	kg m^2
I_y	Pitch inertia moment	kg m^2
$K_i\ (i=fl,fr,rl,rr)$	Stiffness of car body spring	N/m
$K_{ti}\ (i=fl,fr,rl,rr)$	Tire stiffness	N/m
l_f	Distance from COG to front wheel	m
l_r	Distance from COG to rear wheel	m
l_w	Half treat	m
m_s	Total sprung mass	kg
$m_{si}\ (i=fl,fr,rl,rr)$	Sprung mass in each wheel	kg
$m_{ui}\ (i=fl,fr,rl,rr)$	Unsprung mass	kg
$z_{ri}\ (i=fl,fr,rl,rr)$	Road disturbance	m
$z_s\ (i=fl,fr,rl,rr)$	Sprung vertical displacement	m
$z_{ui}\ (i=fl,fr,rl,rr)$	Unsprung vertical displacement	m

As the irregularities of the road are not measured, they are unknown. Therefore, they can be considered disturbances to

This article has been accepted for publication in a future issue of this journal, but has not been fully edited. Content may change prior to final publication. Citation information: DOI 10.1109/TMECH.2019.2909977, IEEE/ASME Transactions on Mechatronics

the vehicle dynamics. Assuming that these disturbances are the result of white noise we then can consider that:

$$\ddot{z}_{rfl} = \quad \ddot{z}_{rfr} = \quad \ddot{z}_{rrl} = \quad \ddot{z}_{rrr} = \quad 0 \tag{6}$$

and they now are evaluated as states instead of inputs.

IV. State-space vehicle model

The complete suspension vehicle model is represented in the time domain by means of a continuous time state-space model:

$$\begin{aligned} \dot{\mathbf{x}} &= \mathbf{A}\mathbf{x} + \mathbf{w} \\ \mathbf{y} &= \mathbf{D}\mathbf{x} + \mathbf{F} + \mathbf{v} \end{aligned} \tag{7}$$

where $\mathbf{x}$=[ϕ, θ, z_s, z_{ufl}, z_{ufr}, z_{url}, z_{urr}, $\dot{\phi}$, $\dot{\theta}$, $\dot{z}_s$, $\dot{z}_{ufl}$, $\dot{z}_{ufr}$, $\dot{z}_{url}$, $\dot{z}_{urr}$, z_{rfl}, z_{rfr}, z_{rrl}, z_{rrr}, $\dot{z}_{rfl}$, $\dot{z}_{rfr}$, $\dot{z}_{rrl}$, $\dot{z}_{rrr}$] is the state vector, $\mathbf{y}$=[$\ddot{z}_s$, z_s, $z_{sfl} - z_{ufl}$, $z_{sfr} - z_{ufr}$, $z_{srl} - z_{url}$, $z_{srr} - z_{urr}$, $compression_{fl}$, $compression_{fr}$, $compression_{rl}$, $compression_{rr}$] is the output vector, where $compression_i$ is the real data given by the suspension deflection sensors mounted on each vehicle damper. The use of the suspension deflection sensors is necessary in order to estimate the vehicle mass even though the vehicle is stopped. The value of $compression_i$ represents the deflection suspension related to the static equilibrium position, then:

$$compression_i = z_{si} - z_{ui} - \frac{m_{si}}{K_{si}} g \quad \text{for i=fl,fr,rl,rr} \tag{8}$$

In a first approximation, we can consider that the mass which actuates in each suspension is given by:

$$m_{sfl} = m_{sfr} = \tfrac{m_s l_r}{2(l_f + l_r)}; \quad m_{srl} = m_{srr} = \tfrac{m_s l_f}{2(l_f + l_r)} \tag{9}$$

Matrices $\mathbf{A}$, $\mathbf{D}$ and $\mathbf{F}$ are given in Appendix A. Finally, $\mathbf{w}$ and $\mathbf{v}$ are the state disturbance and the observation noise vectors, respectively, which are assumed to be Gaussian, uncorrelated and zero mean: $\mathbf{w} \sim N(0, \mathbf{Q})$ and $\mathbf{v} \sim N(0, \mathbf{R})$, where $\mathbf{Q}$ is the covariance matrix of the process noise and $\mathbf{R}$ is the covariance matrix of the measurement noise.

The continuous state-space system of equation (7) is transformed to a discrete one using the first order approximation of Euler $\dot{\mathbf{x}}_{k-1} = \frac{\mathbf{x}_k - \mathbf{x}_{k-1}}{T_s}$, where T_s is the sampling time. Therefore, the discrete system can be expressed as:

$$\begin{aligned} \mathbf{x}_k &= \mathbf{A}_d \mathbf{x}_{k-1} + \mathbf{B}_d \mathbf{u}_{k-1} + \mathbf{w}_{k-1} \\ \mathbf{y}_k &= \mathbf{D}\mathbf{x}_k + \mathbf{F} + \mathbf{v}_k \end{aligned} \tag{10}$$

where $\mathbf{A}_d$=($\mathbf{I}$+T$_s\mathbf{A}$) and $\mathbf{y}_k$=[$\ddot{z}_{s,k}$, $z_{s,k}$, $z_{sfl,k} - z_{ufl,k}$, $z_{sfr,k} - z_{ufr,k}$, $z_{srl,k} - z_{url,k}$, $z_{srr,k} - z_{urr,k}$, $compression_{fl,k}$, $compression_{fr,k}$, $compression_{rl,k}$, $compression_{rr,k}$] is the sensor data used in each step k.

V. Dual Kalman filter

A DKF is used in this work in order to estimate both road irregularities and vehicle mass. As for mass, it is calculated as the sum of unsprung mass (m$_{ui}$) and sprung mass (m$_s$). In a real vehicle, unsprung masses do not change. Therefore, the estimation of its mass will consist of estimating the sprung mass.

The design of a vehicle model which allows the mass to be estimated not only in dynamic conditions but also in static ones is very successful because an accurate value of this mass can be obtained more quickly. Additionally, we can consider that the loading and unloading of items and passengers onto a vehicle is carried out when the vehicle is stopped or its velocity is very slow. Taking into account this fact, it would be interesting if the mass estimation algorithm could be disconnected when the estimated mass does not change significantly in each iteration in order to reduce the computing time. For this reason, a DKF has been selected for such purpose.

A DKF is formed by two independent Kalman filters. One of them is called Kalman state and the other is called Kalman parameter. At each iteration, states are estimated using the current estimated parameters, and parameters are estimated using the previous estimated states. The DKF algorithm is given by the following recursive steps [31]:

1) Parameter prediction:

$$\tilde{\mathbf{x}}_{p,k|k-1} = \tilde{\mathbf{x}}_{p,k-1|k-1} \tag{11}$$

$$\mathbf{P}_{p,k|k-1} = \mathbf{P}_{p,k-1|k-1} + \mathbf{Q}_p \tag{12}$$

2) State prediction:

$$\tilde{\mathbf{x}}_{s,k|k-1} = \mathbf{A}_d \left(\tilde{\mathbf{x}}_{p,k|k-1}\right) \tilde{\mathbf{x}}_{s,k-1|k-1} \tag{13}$$

$$\mathbf{P}_{s,k|k-1} = \mathbf{A}_d \left(\tilde{x}_{p,k|k-1}\right) \mathbf{P}_{s,k-1|k-1} \mathbf{A}_d \left(\tilde{\mathbf{x}}_{p,k|k-1}\right)^T + \mathbf{Q}_s \tag{14}$$

3) State correction:

$$\mathbf{K}_{s,k} = \mathbf{P}_{s,k|k-1} + \mathbf{C}^T \left[\mathbf{C}\mathbf{P}_{s,k|k-1}\mathbf{C}^T + \mathbf{R}_s\right]^{-1} \tag{15}$$

$$\tilde{\mathbf{x}}_{s,k|k} = \tilde{\mathbf{x}}_{s,k|k-1} + \underline{\mathrm{K}}_{s,k} \left[\mathbf{y}_{obs} - \mathbf{C}\tilde{\mathbf{x}}_{s,k|k-1}\right] \tag{16}$$

$$\mathbf{P}_{s,k|k} = \left[\mathbf{I} - \mathbf{K}_{s,k}\mathbf{C}\right] \mathbf{P}_{s,k|k-1} \tag{17}$$

4) Parameter correction:

$$\mathbf{K}_{p,k} = \mathbf{P}_{p,k|k-1} + J^T \left[J\mathbf{P}_{p,k|k-1}J^T + \mathbf{R}_p\right]^{-1} \tag{18}$$

$$\mathbf{y}_{est} = \mathbf{A}_d \left(\tilde{\mathbf{x}}_{p,k|k-1}\right) \tilde{\mathbf{x}}_{s,k|k} \tag{19}$$

$$\tilde{\mathbf{x}}_{p,k|k} = \tilde{\mathbf{x}}_{p,k|k-1} + \mathbf{K}_{p,k} \left[\mathbf{y}_{obs} - \mathbf{y}_{est}\right] \tag{20}$$

$$\mathbf{P}_{p,k|k} = \left[\mathbf{I} - \mathbf{K}_{p,k}J\right] \mathbf{P}_{p,k|k-1} \tag{21}$$

where $\tilde{\mathbf{x}}_{p,k} = [m_s]$ is the parameter vector, $\tilde{\mathbf{x}}_{s,k}$ =[ϕ, θ, z_s, z_{ufl}, z_{ufr}, z_{url}, z_{urr}, $\dot{\phi}$, $\dot{\theta}$, $\dot{z}_s$, $\dot{z}_{ufl}$, $\dot{z}_{ufr}$, $\dot{z}_{url}$, $\dot{z}_{urr}$] is the state vector, $\mathbf{P_s}$ and $\mathbf{P_p}$ are the error covariance matrices and $\mathbf{K_s}$ and $\mathbf{K_p}$ are the Kalman gain matrices, for states and parameters, respectively. $\mathbf{H_s} = \mathbf{D}$ and $\mathbf{H_p}$ is the Jacobian matrix of parameter estimator given by:

$$\begin{aligned} \mathbf{H_p} = \; & [\tfrac{\partial \ddot{z}_s}{\partial m_s}; \tfrac{\partial z_s}{\partial m_s}; \tfrac{\partial (z_{sfl} - z_{ufl})}{\partial m_s}; \tfrac{\partial (z_{sfr} - z_{ufr})}{\partial m_s}; \tfrac{\partial (z_{srl} - z_{url})}{\partial m_s}; \\ & \tfrac{\partial (z_{srr} - z_{urr})}{\partial m_s}; \tfrac{\partial (compresion_{ufl})}{\partial m_s}; \tfrac{\partial (compresion_{ufl})}{\partial m_s}; \\ & \tfrac{\partial (compresion_{ufr})}{\partial m_s}; \tfrac{\partial (compresion_{url})}{\partial m_s}; \tfrac{\partial (compresion_{urr})}{\partial m_s}] \end{aligned} \tag{22}$$

Both parameter and state Kalman filters depend on the same output. Then, their observation noise covariances are the same:

$$\begin{aligned} \mathbf{R_s} = \mathbf{R_p} = \; & diag[\sigma^2_{\ddot{z}_s}; \sigma^2_{z_s}; \sigma_{z_{sfl} - z_{ufl}}; \sigma_{z_{sfr} - z_{ufr}}; \\ & \sigma_{z_{srl} - z_{url}}; \sigma_{z_{srr} - z_{urr}}; \sigma^2_{compresion_{fl}}; \\ & \sigma^2_{compresion_{fr}}; \sigma^2_{compresion_{rf}}; \sigma^2_{compresion_{rr}}]; \end{aligned} \tag{23}$$

This article has been accepted for publication in a future issue of this journal, but has not been fully edited. Content may change prior to final publication. Citation information: DOI 10.1109/TMECH.2019.2909977, IEEE/ASME Transactions on Mechatronics

The process noise covariance matrix of state estimator is given by:

$$Q_s = R_0 I \tag{24}$$

where R_0 is a large value. In our experiments R_0 is equal to 1000000. The process noise covariance matrix of parameter estimator is given by:

$$Q_p = \sigma_{m_s}^2 \tag{25}$$

where σ_{m_s} is about 1% of the corresponding initial value of vehicle sprung mass.

VI. Simulated and Experimental Results

The performance of the designed state/parameter observer has been validated for two types of vehicle configurations: a C-Class Hatchback and a van. They have been modeled through the CarSim and TruckSim softwares, respectively, connected to a Simulink model which provides a graphical interface for integrating the MATLAB function block. The MATLAB block was used to implement the proposed DKF algorithm. Additionally, the van model in Trucksim has been validated using sensor data obtained from a real van Mercedes Sprinter Vito (see Figure 3). Results regarding this validation can be found in [30].

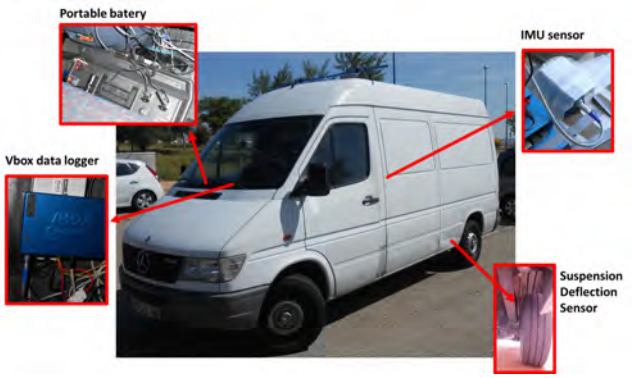

Fig. 3: Real van: Mercedes Vito for experiments

In Table II, the values of the parameters used for the state space system are listed.

TABLE II: Values of vehicle parameters for the state space system

	C-Class Hatchback	Van
C_i $(i = fl, fr, rl, rr)$	2923.74 Ns/m	1554.47 Ns/m
I_x	606.1 kg/m^2	500 kg/m^2
I_y	1523 kg/m^2	2975 kg/m^2
K_i $(i = fl, fr, rl, rr)$	228000 Nm	750000 Nm
l_f	1.016 m	1.5096 m
l_r	1.562 m	2.0404 m
l_w	1.539 m	1.638 m
m_{ui} $(i = fl, fr, rl, rr)$	35.5 kg	100 kg
m_s	1274 kg	1700 kg

Different simulation driving tests for both vehicle configurations are carried out in order to prove the performance of the proposed vehicle. The C-Class Hatchback is evaluated in the following maneuvering scenarios:

- J-turn maneuver at 30 km/h with a steering wheel angle of -75 deg and a friction coefficient of 1.0.
- J-turn maneuver at 100 km/h with a steering wheel angle of -125 deg and a friction coefficient of 1.0.
- Straight maneuver with roughness at 100 km/h and friction coefficients of 0.3 and 1.0. The road profile is depicted in Figure 4a.
- Straight maneuver with roughness at 40 km/h, friction coefficient of 0.9 and slope of 36%.
- Straight maneuver with a small bump and roughness at 100 km/h and a friction coefficient of 0.85. The road profile is depicted in Figure 4b.
- Double Lane Change (DLC) maneuver at 50 km/h and a friction coefficient of 0.85.
- DLC maneuver at 120 km/h and a friction coefficient of 0.85.
- Bounce sine sweep test at 40 km/h and a friction coefficient of 0.85. The road profile is depicted in Figure 4c.

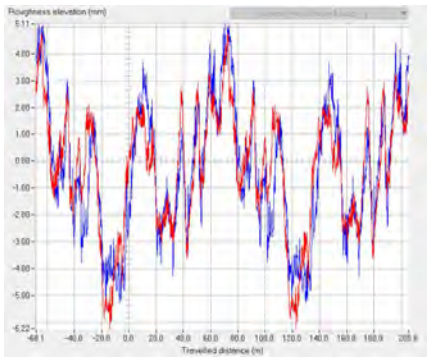

(a) Roughness profile

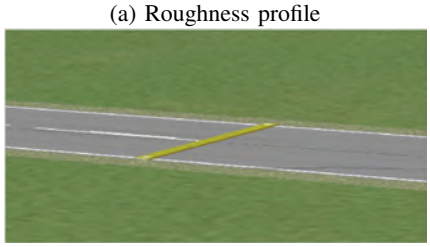

(b) Roughness road with a small bump

(c) Bounce sine sweep test

Fig. 4: Road profiles used for simulations

To prove the performance of the proposed algorithm, we analyze the relative error and convergence to the real value of sprung mass for the C-Class Hatchback (1274 kg, see Table II). Figure 5 shows the variation of sprung mass estimation and its relative error for each maneuver considering a sprung mass initial value of 5000 kg. Analyzing the results for the proposed method based on DKF as is shown in Table III,

This article has been accepted for publication in a future issue of this journal, but has not been fully edited. Content may change prior to final publication. Citation information: DOI 10.1109/TMECH.2019.2909977, IEEE/ASME Transactions on Mechatronics

TABLE III: C-Class Hatchback: error and convergence time

Maneuvering scenarios	RLS method		Proposed method based on DKF	
	Error (%)	Convergence time (seconds)	Error (%)	Convergence time (seconds)
Bounce sine sweep test at 40 km/h with μ=0.85 (duration 0 -19 seconds)	$\approx$ 188	$\approx$ 16	>50	-
DLC at 50 km/h with μ=0.85	$\approx$ 16	$\approx$ 20	<5	<1
DLC at 120 km/h with μ=0.85	$\approx$ 15	$\approx$ 5.5	<5	<1
J-turn at 30 km/h with μ=1	$\approx$ 100	-	<5	<1
J-turn at 100 km/h with μ=1	$\approx$ 110	$\approx$ 18	>50	-
Straight line at 40 km/h with a small sharp bump and roughness and μ=0.85	$\approx$ 250	$\approx$ 17	<5	<1
Straight line at 100 km/h with roughness and μ=1	$\approx$ 22	$\approx$ 13	<5	<1
Straight line at 100 km/h with roughness and μ=0.3	$\approx$ 25	<1	<5	<1
Straight line at 40 km/h with roughness and μ=0.9 and slope 36%	$\approx$ 20	<5	<1	$\approx$ 1

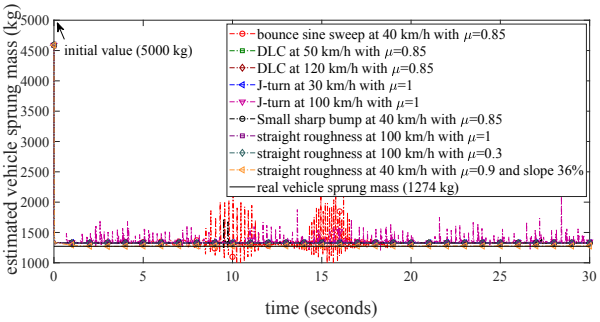

(a) Evolution of the vehicle sprung mass estimates

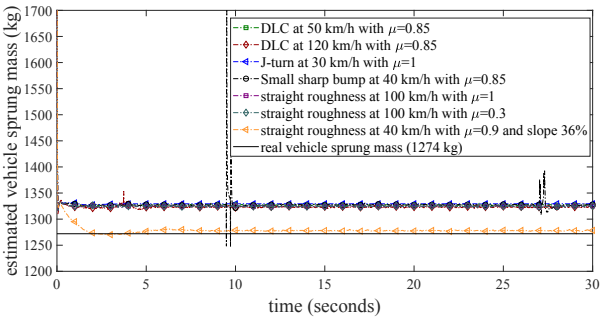

(b) Zoom of Figure 5a

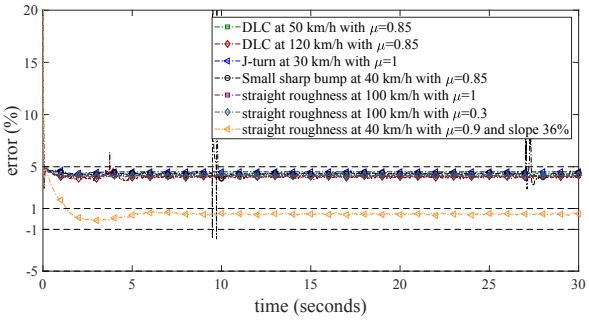

(c) Relative error

Fig. 5: C-Class Hatchback: simulation results for different driving maneuvers

it can be observed that the sprung mass reaches its real value with a relative error of $< 5\%$ in one second for the majority of maneuvers with different friction coefficients and road grades. For a smooth maneuver such as straight line at 40 km/h with roughness, the relative error is $< 1\%$. For very severe maneuvers such as a bounce sine sweep test at 40 km/h and J-turn at 100 km/h, the algorithm does not work properly. To solve this situation, a supervisor could be designed to switch off the mass estimation KF block once high accelerations are detected. Additionally, results obtained using the classical RLS method are depicted in Table III. The RLS method estimates the sprung mass through equation (3). As example, Figure 6 shows the comparison between the proposed method based on DKF and the RLS one for a DLC maneuver at 120 km/h with μ=0.85. Results show that the proposed method has a better performance than the RLS one. Figure 7 shows the estimated and real irregularities for a straight line maneuver at 100 km/h and 40 km/h with roughness and a small sharp bump, respectively. It can be seen that the irregularities estimation strongly depends on a good sprung mass estimation. At the beginning of the simulation, the mass estimation is not suitable, nor is the estimation of road irregularities. As for a small sharp bump, the algorithm correctly detects the beginning and the end of the bump (see Figure 7a).

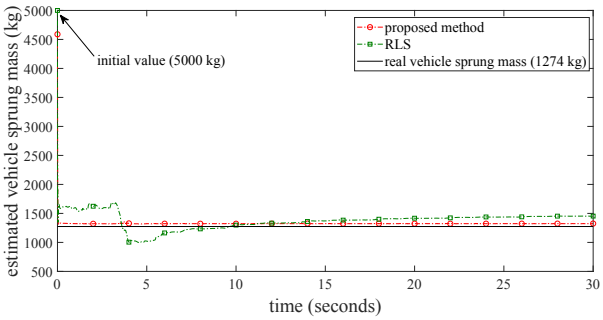

Fig. 6: C-Class Hatchback: comparison between the proposed method based on DKF and the RLS one for a DLC maneuver at 120 km/h with μ=0.85

For the simulated van, two driving tests are carried out. The first case takes into account that the van is unloaded and the second one considers that it is loaded with 500 kg for a straight maneuver at 100 km/h with road roughness. Figures 8 and 9 show the variation of sprung mass for the unloaded van and the van loaded with 500 kg, respectively. The sprung mass converges to around 1840 kg and 2400 kg, respectively. Compared to the real values, 1700 kg and 2200 kg, the relative

This article has been accepted for publication in a future issue of this journal, but has not been fully edited. Content may change prior to final publication. Citation information: DOI 10.1109/TMECH.2019.2909977, IEEE/ASME Transactions on Mechatronics

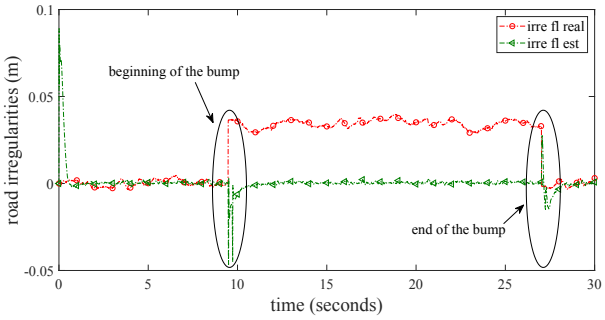

(a) Small sharp bump at 40 km/h

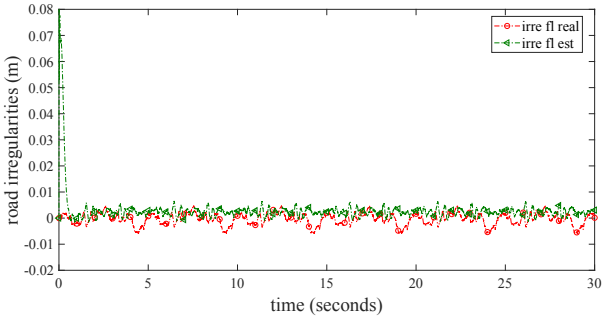

(b) Straight roughness at 100 km/h with μ=0.3

Fig. 7: C-Class Hatchback: Estimated road profile

error is about 8% and 9%, respectively.

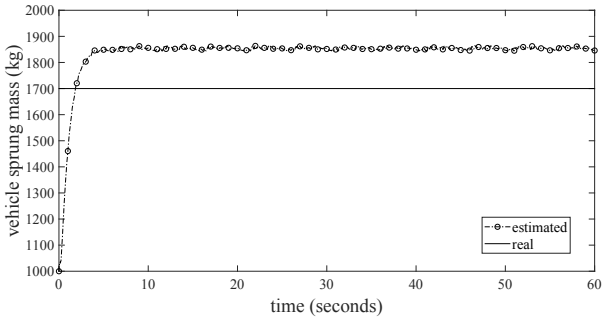

(a) Sprung mass estimation

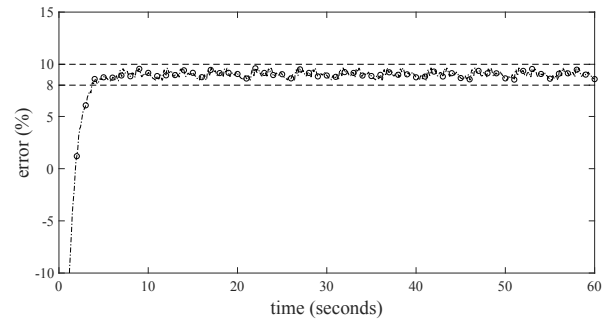

(b) Relative error

Fig. 8: Unloaded van

Finally, experiments were performed using an experimental testbed composed of a real van, a Mercedes VITO (see Figure 3), equipped with a VBOX 100 Hz data logger enabling the

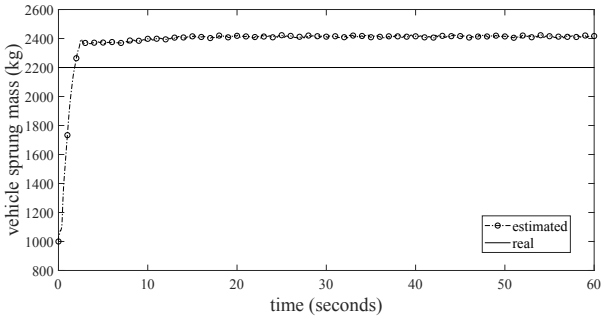

(a) Sprung mass estimation

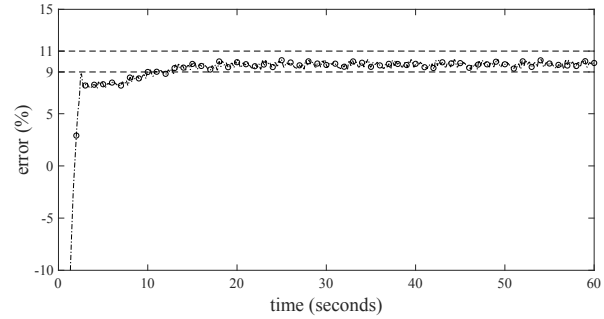

(b) Relative error

Fig. 9: Van loaded with 500 kg

Fig. 10: Real van: Path followed by the real van

synchronization and the evaluation of the logged data provided by an IMU sensor and 4 displacement suspension sensors. The IMU sensor is the Racelogics RLVBIMU04 model. Its provides accurate measurements of 3-axis angular rates and 3-axis accelerations with a resolution of 16 bits ADC, 0.001 deg/s and 0.15 mg, respectively. The IMU was installed close to the vehicle Center of Gravity (COG). In this work, the vertical acceleration is only taken into consideration. The displacement suspension sensors are 2 linear potenciometer sensors, model SA-LP075, for the front suspension, and 2 Linear Variable Differential Transformer (LVDT) sensors, model MTN, for the rear suspension. They were mounted across the vehicles dampers in order to measure the relative suspension displacements.

In Figure 10, the trajectory followed by the van in a real environment is shown. This trajectory is formed by J-turn and slalom maneuvers at a speed from 20 km/h to 50 km/h. Data obtained from the suspension deflection sensors and from the vertical accelerometer are shown in Figures 11a and 11b, respectively. Figures 12a, 12b and 12c show the results for

This article has been accepted for publication in a future issue of this journal, but has not been fully edited. Content may change prior to final publication. Citation information: DOI 10.1109/TMECH.2019.2909977, IEEE/ASME Transactions on Mechatronics

the estimate of sprung mass, the mass relative error and the estimate of the road roughness, respectively. The mean value of the estimated sprung mass is about 1725 kg, with a relative error less than 6% and a convergence time about 11 seconds.

For both the simulations and experiments, the proposed algorithm has been developed in the Matlab environment and performed on a PC with 3.6 GHz Intel Core i7-4790 CPU and 8 GB memory. The computing time for a single cycle is about 0.2 ms, less than the sampling time of data logger (10 ms).

Compared with previous works (see Table IV) in terms of relative error and convergence time, both simulation and experimental tests show that the proposed method has a suitable performance. The main advantages of the proposed method is that it works adequately in both static and dynamic conditions and for different maneuvers even for high speeds and on a slope.

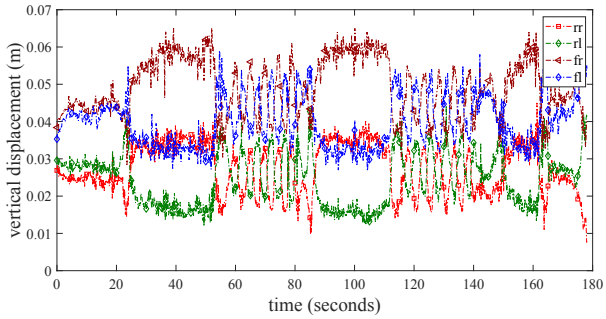

(a) Suspension deflections

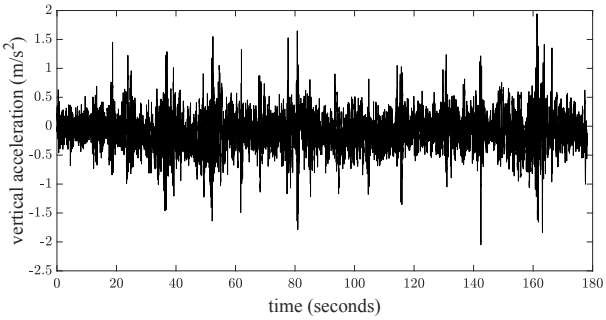

(b) Vertical acceleration

Fig. 11: Real van: Sensor data

VII. Conclusion and Future Work

This paper proposes a state-parameter observer that allows the vehicle mass to be estimated under static and dynamic driving vehicle conditions using measurements of sensors which can be mounted easily on vehicles. A DKF based on a vertical complete vehicle model is considered for vehicle mass and road irregularities estimation using the data obtained from a suspension deflection sensors and a vertical accelerometer. The advantage of this method is that it can be used under static and dynamic driving conditions. Both simulation and experimental results are carried out to prove the effectiveness of the proposed algorithm. From these results we can observe that the convergence of the algorithm depends on the type of vehicle considered. In an automobile, the

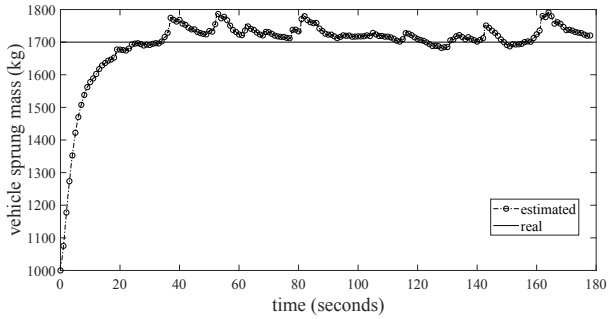

(a) Vehicle sprung mass

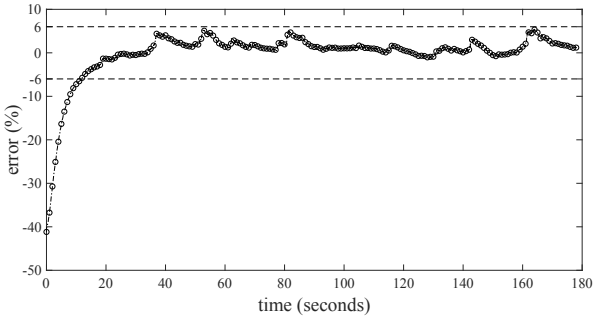

(b) Vehicle sprung mass error

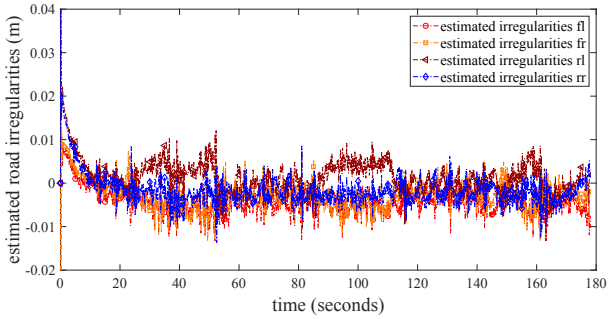

(c) Estimated road roughness

Fig. 12: Real van: Experimental results

errors obtained ($< 5\%$) and convergence time (< 1 second) are lower than those obtained in previous works for normal driving conditions. In a light commercial vehicle (van), the maximum relative error obtained during real maneuvers is about 6% with a time convergence of 11 seconds. Future works will focus on 1) designing a supervisor to switch off the mass estimation KF block once high accelerations are detected and 2) designing a robust controller for the vehicle performance improvement considering the estimated mass into the definition of scheduling variables.

Appendix A

Matrices **A**, **D** and **F** are defined in equations (26), (27) and (28), where:

$$a_{8,1} = \frac{(-K_{fl}-K_{fr}-K_{rl}-K_{rr})}{I_x} l_w l_w$$

$$a_{8,2} = \frac{(-K_{fl}l_f+K_{fr}l_f+K_{rl}l_r-K_{rr}l_r)}{I_x} l_w$$

$$a_{8,3} = \frac{(-K_{fl}+K_{fr}-K_{rl}+K_{rr})}{I_x} l_w$$

This article has been accepted for publication in a future issue of this journal, but has not been fully edited. Content may change prior to final publication. Citation information: DOI 10.1109/TMECH.2019.2909977, IEEE/ASME Transactions on Mechatronics

TABLE IV: Comparison of previous methods for the vehicle mass estimation

	Maneuver	**Simulation / Experiments**	**Model**	**Relative error (%)**	**Convergence time (s)**	**Limitations**
Wenzel et al. [16]	Combined acceleration, braking and cornering at low speed	Both	Lateral-longitudinal four-wheel vehicle	≈4 Magic Formula tyre model ≈20 TMeasy tyre model	>40	Dynamic conditions. Highly dependent of the tyre model
Fathy et al. [17]	Acceleration and braking	Both	Longitudinal vehicle model	≈4	>50	Dynamic conditions. Small grade. Estimation is only carried out in conditions of ”significant, predominantly longitudinal motion
Maleej et al. [18]	Acceleration at maximum velocity of 40 km/h	Experiments	Electric vehicle with longitudinal dynamics	<3	≈5	Dynamic conditions. No estimation is performed in cruise, deceleration and stop states. Flat road
Hong et al. [19]	Combined acceleration, braking and cornering at maximum velocity of 55 km/h	Both	Lateral-longitudinal four-wheel vehicle model	≈0.5	>20	Dynamic conditions. Estimation is performed under the prevailing longitudinal dynamics. Estimation of a mass added on the vehicle
Jordan et al. [20]	80 km/h	Experimental	Simplified vehicle model	>15	≈20	Dynamic conditions. No pitch and roll motions considered.

$$
\mathbf{A}=\begin{bmatrix}
0 & 0 & 0 & 0 & 0 & 0 & 0 & 1 & 0 & 0 & 0 & 0 & 0 & 0 & 0 & 0 & 0 & 0 & 0 & 0 & 0 & 0\\
0 & 0 & 0 & 0 & 0 & 0 & 0 & 0 & 1 & 0 & 0 & 0 & 0 & 0 & 0 & 0 & 0 & 0 & 0 & 0 & 0 & 0\\
0 & 0 & 0 & 0 & 0 & 0 & 0 & 0 & 0 & 1 & 0 & 0 & 0 & 0 & 0 & 0 & 0 & 0 & 0 & 0 & 0 & 0\\
0 & 0 & 0 & 0 & 0 & 0 & 0 & 0 & 0 & 0 & 1 & 0 & 0 & 0 & 0 & 0 & 0 & 0 & 0 & 0 & 0 & 0\\
0 & 0 & 0 & 0 & 0 & 0 & 0 & 0 & 0 & 0 & 0 & 1 & 0 & 0 & 0 & 0 & 0 & 0 & 0 & 0 & 0 & 0\\
0 & 0 & 0 & 0 & 0 & 0 & 0 & 0 & 0 & 0 & 0 & 0 & 1 & 0 & 0 & 0 & 0 & 0 & 0 & 0 & 0 & 0\\
0 & 0 & 0 & 0 & 0 & 0 & 0 & 0 & 0 & 0 & 0 & 0 & 0 & 1 & 0 & 0 & 0 & 0 & 0 & 0 & 0 & 0\\
a_{8,1} & a_{8,2} & a_{8,3} & a_{8,4} & a_{8,5} & a_{8,6} & a_{8,7} & a_{8,8} & a_{8,9} & a_{8,10} & a_{8,11} & a_{8,12} & a_{8,13} & a_{8,14} & 0 & 0 & 0 & 0 & 0 & 0 & 0 & 0\\
a_{9,1} & a_{9,2} & a_{9,3} & a_{9,4} & a_{9,5} & a_{9,6} & a_{9,7} & a_{9,8} & a_{9,9} & a_{9,10} & a_{9,11} & a_{9,12} & a_{9,13} & a_{9,14} & 0 & 0 & 0 & 0 & 0 & 0 & 0 & 0\\
a_{10,1} & a_{10,2} & a_{10,3} & a_{10,4} & a_{10,5} & a_{10,6} & a_{10,7} & a_{10,8} & a_{10,9} & a_{10,10} & a_{10,11} & a_{10,12} & a_{10,13} & a_{10,14} & 0 & 0 & 0 & 0 & 0 & 0 & 0 & 0\\
a_{11,1} & a_{11,2} & a_{11,3} & a_{11,4} & 0 & 0 & 0 & a_{11,8} & a_{11,9} & a_{11,10} & a_{11,11} & 0 & 0 & 0 & a_{11,15} & 0 & 0 & 0 & 0 & 0 & 0 & 0\\
a_{12,1} & a_{12,2} & a_{12,3} & 0 & a_{12,5} & 0 & 0 & a_{12,8} & a_{12,9} & a_{12,10} & 0 & a_{12,12} & 0 & 0 & 0 & a_{12,16} & 0 & 0 & 0 & 0 & 0 & 0\\
a_{13,1} & a_{13,2} & a_{13,3} & 0 & 0 & a_{13,6} & 0 & a_{13,8} & a_{13,9} & a_{13,10} & 0 & 0 & a_{13,13} & 0 & 0 & 0 & a_{13,17} & 0 & 0 & 0 & 0 & 0\\
a_{14,1} & a_{14,2} & a_{14,3} & 0 & 0 & 0 & a_{14,7} & a_{14,8} & a_{14,9} & a_{14,10} & 0 & 0 & 0 & a_{14,14} & 0 & 0 & 0 & a_{14,18} & 0 & 0 & 0 & 0\\
0 & 0 & 0 & 0 & 0 & 0 & 0 & 0 & 0 & 0 & 0 & 0 & 0 & 0 & 0 & 0 & 0 & 0 & 1 & 0 & 0 & 0\\
0 & 0 & 0 & 0 & 0 & 0 & 0 & 0 & 0 & 0 & 0 & 0 & 0 & 0 & 0 & 0 & 0 & 0 & 0 & 1 & 0 & 0\\
0 & 0 & 0 & 0 & 0 & 0 & 0 & 0 & 0 & 0 & 0 & 0 & 0 & 0 & 0 & 0 & 0 & 0 & 0 & 0 & 1 & 0\\
0 & 0 & 0 & 0 & 0 & 0 & 0 & 0 & 0 & 0 & 0 & 0 & 0 & 0 & 0 & 0 & 0 & 0 & 0 & 0 & 0 & 1\\
0 & 0 & 0 & 0 & 0 & 0 & 0 & 0 & 0 & 0 & 0 & 0 & 0 & 0 & 0 & 0 & 0 & 0 & 0 & 0 & 0 & 0\\
0 & 0 & 0 & 0 & 0 & 0 & 0 & 0 & 0 & 0 & 0 & 0 & 0 & 0 & 0 & 0 & 0 & 0 & 0 & 0 & 0 & 0\\
0 & 0 & 0 & 0 & 0 & 0 & 0 & 0 & 0 & 0 & 0 & 0 & 0 & 0 & 0 & 0 & 0 & 0 & 0 & 0 & 0 & 0\\
0 & 0 & 0 & 0 & 0 & 0 & 0 & 0 & 0 & 0 & 0 & 0 & 0 & 0 & 0 & 0 & 0 & 0 & 0 & 0 & 0 & 0
\end{bmatrix} \tag{26}
$$

$$
\mathbf{D}=\begin{bmatrix}
d_{1,1} & d_{1,2} & d_{1,3} & d_{1,4} & d_{1,5} & d_{1,6} & d_{1,7} & d_{1,8} & d_{1,9} & d_{1,10} & d_{1,11} & d_{1,12} & d_{1,13} & d_{1,14} & 0 & 0 & 0 & 0 & 0 & 0 & 0 & 0\\
d_{3,1} & d_{3,2} & 1 & -1 & 0 & 0 & 0 & 0 & 0 & 0 & 0 & 0 & 0 & 0 & 0 & 0 & 0 & 0 & 0 & 0 & 0 & 0\\
d_{4,1} & d_{4,2} & 1 & 0 & -1 & 0 & 0 & 0 & 0 & 0 & 0 & 0 & 0 & 0 & 0 & 0 & 0 & 0 & 0 & 0 & 0 & 0\\
d_{5,1} & d_{5,2} & 1 & 0 & 0 & -1 & 0 & 0 & 0 & 0 & 0 & 0 & 0 & 0 & 0 & 0 & 0 & 0 & 0 & 0 & 0 & 0\\
d_{6,1} & d_{6,2} & 1 & 0 & 0 & 0 & -1 & 0 & 0 & 0 & 0 & 0 & 0 & 0 & 0 & 0 & 0 & 0 & 0 & 0 & 0 & 0\\
d_{7,1} & d_{7,2} & 1 & -1 & 0 & 0 & 0 & 0 & 0 & 0 & 0 & 0 & 0 & 0 & 0 & 0 & 0 & 0 & 0 & 0 & 0 & 0\\
d_{8,1} & d_{8,2} & 1 & 0 & -1 & 0 & 0 & 0 & 0 & 0 & 0 & 0 & 0 & 0 & 0 & 0 & 0 & 0 & 0 & 0 & 0 & 0\\
d_{9,1} & d_{9,2} & 1 & 0 & 0 & -1 & 0 & 0 & 0 & 0 & 0 & 0 & 0 & 0 & 0 & 0 & 0 & 0 & 0 & 0 & 0 & 0\\
d_{10,1} & d_{10,2} & 1 & 0 & 0 & 0 & -1 & 0 & 0 & 0 & 0 & 0 & 0 & 0 & 0 & 0 & 0 & 0 & 0 & 0 & 0 & 0
\end{bmatrix} \tag{27}
$$

$$
\mathbf{F}=\begin{bmatrix} 0 & 0 & 0 & 0 & 0 & 0 & -\frac{m_{sfl}}{K_{fl}}g & -\frac{m_{sfr}}{K_{fr}}g & -\frac{m_{srl}}{K_{rl}}g & -\frac{m_{srr}}{K_{rr}}g \end{bmatrix}^T \tag{28}
$$

$a_{8,4}=-\frac{K_{fl}l_w}{I_x};\ a_{8,5}=\frac{K_{fr}l_w}{I_x};\ a_{8,6}=-\frac{K_{rl}l_w}{I_x}I_x$ $\quad a_{8,9}=\frac{(-C_{fl}l_f+C_{fr}l_f+C_{rl}l_r-C_{rr}l_r)}{I_x}l_w$

$a_{8,7}=\frac{K_{rr}l_w}{I_x};\ a_{8,8}=\frac{(-C_{fl}-C_{fr}-C_{rl}-C_{rr})}{I_x}l_wl_w$ $\quad a_{8,10}=\frac{(-C_{fl}+C_{fr}-C_{rl}+C_{rr})}{I_x}l_w;\ a_{8,11}=-\frac{C_{fl}l_w}{I_x}$

$$a_{8,12}=\frac{C_{fr}l_w}{I_x};\ a_{8,13}=-\frac{C_{rl}l_w}{I_x};\ a_{8,14}=\frac{C_{rr}l_w}{I_x}$$

$$a_{9,1}=\frac{(-K_{fl}l_f+K_{fr}l_f+K_{rl}l_r-K_{rr}l_r)}{I_y}l_w$$

$$a_{9,2}=\frac{(-K_{fl}l_fl_f-K_{fr}l_fl_f-K_{rl}l_rl_r-K_{rr}l_rl_r)}{I_y}$$

$$a_{9,3}=\frac{(K_{fl}l_f+K_{fr}l_f-K_{rl}l_r-K_{rr}l_r)}{I_y}$$

$$a_{9,4}=-\frac{K_{fl}l_f}{I_y};\ a_{9,5}=-\frac{K_{fr}l_f}{I_y};\ a_{9,6}=\frac{K_{rl}l_r}{I_y}$$

$$a_{9,7}=\frac{K_{rr}l_r}{I_y};\ a_{9,8}=\frac{(-C_{fl}l_f+C_{fr}l_f+C_{rl}l_r-C_{rr}l_r)}{I_y}l_w$$

$$a_{9,9}=\frac{(-C_{fl}l_fl_f-C_{fr}l_fl_f-C_{rl}l_rl_r-C_{rr}l_rl_r)}{I_y}$$

$$a_{9,10}=\frac{(C_{fl}l_f+C_{fr}l_f-C_{rl}l_r-C_{rr}l_r)}{I_y}$$

$$a_{9,11}=-\frac{C_{fl}l_f}{I_y};\ a_{9,12}=-\frac{C_{fr}l_f}{I_y};\ a_{9,13}=\frac{C_{rl}l_r}{I_y}$$

$$a_{9,14}=\frac{C_{rr}l_r}{I_y};\ a_{10,1}=\frac{(K_{fl}-K_{fr}-K_{rl}+K_{rr})}{m_s}l_w$$

$$a_{10,2}=\frac{(K_{fl}l_f+K_{fr}l_f-K_{rl}l_r-K_{rr}l_r)}{m_s}$$

$$a_{10,3}=\frac{(-K_{fl}-K_{fr}-K_{rl}-K_{rr})}{m_s};\ a_{10,4}=\frac{K_{fl}}{m_s};$$

$$a_{10,5}=\frac{K_{fr}}{m_s};\ a_{10,6}=\frac{K_{rl}}{m_s};\ a_{10,7}=\frac{K_{rr}}{m_s}$$

$$a_{10,8}=\frac{(C_{fl}-C_{fr}-C_{rl}+C_{rr})}{m_s}l_w$$

$$a_{10,9}=\frac{(-C_{fl}l_f+C_{fr}l_f-C_{rl}l_r-C_{rr}l_r)}{m_s}$$

$$a_{10,10}=\frac{(-C_{fl}-C_{fr}-C_{rl}-C_{rr})}{m_s};\ a_{10,11}=\frac{C_{fl}}{m_s}$$

$$a_{10,12}=\frac{C_{fr}}{m_s};\ a_{10,13}=\frac{C_{rl}}{m_s};\ a_{10,14}=\frac{C_{rr}}{m_s}$$

$$a_{11,1}=-\frac{K_{fl}l_w}{m_{ufl}};\ a_{11,2}=-\frac{K_{fl}l_f}{m_{ufl}};\ a_{11,3}=\frac{K_{fl}}{m_{ufl}}$$

$$a_{11,4}=-\frac{(K_{fl}+K_{ufl})}{m_{ufl}};\ a_{11,8}=-\frac{C_{fl}l_w}{m_{ufl}};\ a_{11,9}=-\frac{C_{fl}l_f}{m_{ufl}}$$

$$a_{11,10}=\frac{C_{fl}}{m_{ufl}};\ a_{11,11}=-\frac{(C_{fl}+C_{ufl})}{m_{ufl}};\ a_{11,15}=\frac{K_{ufl}}{m_{ufl}}$$

$$a_{12,1}=\frac{K_{fr}l_w}{m_{ufr}};\ a_{12,2}=-\frac{K_{fr}l_f}{m_{ufr}};\ a_{12,3}=\frac{K_{fr}}{m_{ufr}}$$

$$a_{12,5}=-\frac{(K_{fr}+K_{ufr})}{m_{ufr}};\ a_{12,8}=\frac{C_{fr}l_w}{m_{ufr}};\ a_{12,9}=-\frac{C_{fr}l_f}{m_{ufr}}$$

$$a_{12,10}=\frac{C_{fr}}{m_{ufr}};\ a_{12,12}=-\frac{(C_{fr}+C_{ufr})}{m_{ufr}};\ a_{12,16}=\frac{K_{ufr}}{m_{ufr}}$$

$$a_{13,1}=-\frac{K_{rl}l_w}{m_{url}};\ a_{13,2}=\frac{K_{rl}l_r}{m_{url}};\ a_{13,3}=\frac{K_{rl}}{m_{url}}$$

$$a_{13,6}=-\frac{(K_{rl}+K_{url})}{m_{url}};\ a_{13,8}=-\frac{C_{rl}l_w}{m_{url}};\ a_{13,9}=\frac{C_{rl}l_r}{m_{url}}$$

$$a_{13,10}=\frac{C_{rl}}{m_{url}};\ a_{13,13}=-\frac{(C_{rl}+C_{url})}{m_{url}};\ a_{13,17}=\frac{K_{url}}{m_{url}}$$

$$a_{14,1}=\frac{K_{rr}l_w}{m_{urr}};\ a_{14,2}=\frac{K_{rr}l_r}{m_{urr}};\ a_{14,3}=\frac{K_{rr}}{m_{urr}}$$

$$a_{14,7}=-\frac{(K_{rr}+K_{urr})}{m_{urr}};\ a_{14,8}=\frac{C_{rr}l_w}{m_{urr}};\ a_{14,9}=\frac{C_{rr}l_r}{m_{urr}}$$

$$a_{14,10}=\frac{C_{rr}}{m_{urr}};\ a_{14,14}=-\frac{(C_{rr}+C_{urr})}{m_{urr}};\ a_{14,18}=\frac{K_{urr}}{m_{urr}}$$

$$d_{1,1}=a_{10,1};\ d_{1,2}=a_{10,2};\ d_{1,3}=a_{10,3};\ d_{1,4}=a_{10,4}$$

$$d_{1,5}=a_{10,5};\ d_{1,6}=a_{10,6};\ d_{1,7}=a_{10,7};\ d_{1,8}=a_{10,8}$$

$$d_{1,9}=a_{10,9};\ d_{1,10}=a_{10,10};\ d_{1,11}=a_{10,11};\ d_{1,12}=a_{10,12}$$

$$d_{1,13}=a_{10,13};\ d_{1,10}=a_{10,14};\ d_{3,1}=l_f;\ d_{3,2}=l_w$$

$$d_{4,1}=-l_f;\ d_{4,2}=l_w;\ d_{5,1}=l_r;\ d_{5,2}=-l_w;\ d_{6,1}=-l_r$$

$$d_{6,2}=-l_w;\ d_{7,1}=l_f;\ d_{7,2}=l_w;\ d_{8,1}=-l_f;\ d_{8,2}=l_w$$

$$d_{9,1}=l_r;\ d_{9,2}=-l_w;\ d_{10,1}=-l_r;\ d_{10,2}=-l_w$$

ACKNOWLEDGMENT

This work was supported by Projects TRA2008-05373/AUT and TRA2013-48030-C2-1-R from the Spanish Ministry of Economy and Competitiveness.

REFERENCES

[1] Boada, M.J.L.; Boada, B.L.; Castejon, C. and V. Diaz. A fuzzy-based suspension vehicle depending on terrain. *International Journal of Vehicle Design*. **2005**, Vol. 37, N. 4, pp 311-326. doi: 10.1504/IJVD.2005.006597.

[2] Karimi, H.R.; Wang, R.; Zhang, H. and Wang, J. Control and estimation of over-actuated vehicles, *Mechatronics*, **2015**, vol. 30, pp. 259-260. doi: 10.1016/j.mechatronics.2015.08.001.

[3] Riofrio, A.; Sanz, S.; Boada, M.J.L. and Boada, B.L. A LQR-Based Controller with Estimation of Road Bank for Improving Vehicle Lateral and Rollover Stability via Active Suspension. *Sensors*. **2017** 17 (10). doi: 10.3390/s17102318

[4] Nguyen, A.; Sentouh, C. and Popieul, J. Sensor Reduction for Driver-Automation Shared Steering Control via an Adaptive Authority Allocation Strategy. *IEEE/ASME Transactions on Mechatronic*. **2018**, Vol. 23 (1), pp. 5-16. doi: 10.1109/TMECH.2017.2698216

[5] J. C. Tudon-Martinez, C. A. Vivas-Lopez, D. Hernandez-Alcantara, R. Morales-Menendez, O. Sename and R. A. Ramirez-Mendoza. Full Vehicle Combinatory Efficient Damping Controller: Experimental Implementation,*IEEE/ASME Transactions on Mechatronics*. **2018**, Vol. 23, no. 1, pp. 377-388. doi: 10.1109/TMECH.2017.2785127

[6] Zhang, H.; Huang, X.; Wang, J. and Karimi, H.R. Robust energy-to-peak sideslip angle estimation with applications to ground vehicles, *Mechatronics*, **2015**, vol. 30, pp. 338-347. doi: 10.1016/j.mechatronics.2014.08.003.

[7] Zhang, H.; Zhang, G. and J. Wang. $\mathcal{H}_\infty$ Observer Design for LPV Systems With Uncertain Measurements on Scheduling Variables: Application to an Electric Ground Vehicle. *IEEE/ASME Transactions on Mechatronics*. **2016**. Vol. 21, no. 3, pp. 1659-1670. doi: 10.1109/TMECH.2016.2522759

[8] Zhang,H. and Wang, H. Active Steering Actuator Fault Detection for an Automatically-Steered Electric Ground Vehicle. *IEEE Transactions on Vehicular Technology*. **2017**. Vol. 66, no. 5, pp. 3685-3702. doi: 10.1109/TVT.2016.2604759

[9] Jiang. K.; Yan, F. and Zhang, H. Hydrothermal aging factor estimation for two-cell Diesel-engine SCR systems via a dual time-scale unscented Kalman filter. *IEEE Transactions on Industrial Electronics*. **accepted and in press, 2019**. doi: 10.1109/TIE.2019.2896030

[10] Boada, B.L.; Boada, M.J.L.; Vargas-Melendez, L. and Diaz, V. A robust observer based on H∞ filtering with parameter uncertainties combined with Neural Networks for estimation of vehicle roll angle. *Mechanical Systems and Signal Processing*, **2018**, vol. 99, pp 611-623, doi: 10.1016/j.ymssp.2017.06.044.

[11] Xiaoyuan Zhu, X.; Zhang, H.; Yang, B. and Zhang, G. Cloud-based shaft torque estimation for electric vehicle equipped with integrated motor-transmission system, *Mechanical Systems and Signal Processing*, **2018**, vol. 99, pp. 647-660. doi: 10.1016/j.ymssp.2017.07.006.

[12] Nam, K., S.B. Application of Novel Lateral Tire Force Sensors to Vehicle Parameter Estimation of Electric Vehicles. *Sensors*. **2015**. Vol. 15 (11), pp. 28385-28401. doi: 10.3390/s151128385.

[13] Han, K.; Lee, E.; Choi, M. and Choi, S.B. Adaptive Scheme for the Real-Time Estimation of Tire-Road Friction Coefficient and Vehicle Velocity. *IEEE/ASME Transactions on Mechatronics*. **2017**. Vol. 22 (4), pp. 1508-1518. doi: 10.1109/TMECH.2017.2704606.

[14] Jounghee, J.; Dongyoon, H.; Kyoungseok, H. and Choi, S. Real-Time Longitudinal Location Estimation of Vehicle Center of Gravity. *International Journal of Automotive Technology*. **2018**. Vol. 19 (4), pp. 651-658. doi: 10.1007/s12239-018-0062-8.

[15] Reina, G., Paiano, M. and Blanco-Claraco, J.L. Vehicle parameter estimation using a model-based estimator. *Mechanical Systems and Signal Processing*, **2017**, vol. 87 (Part B), pp. 227-241. doi: 10.1016/j.ymssp.2016.06.038.

[16] Wenzel, T.A.; Burnham, K.J.; Blundell, M.V. and Williams, R. A. Dual extended Kalman filter for vehicle state and parameter estimation. *Vehicle System Dynamics*, **2006**, vol. 44 (2), pp. 153-171. doi: 10.1080/00423110500385949.

[17] Fathy, H.K.; Kang, D. and Stein, J.L. Online Vehicle Mass Estimation Using Recursive Least Squares and Supervisory Data Extraction, *Proceedings of the2008 American Control Conference*, **2008**, Seattle, WA, USA, pp. 1842-1848. doi: 10.1109/ACC.2008.4586760

[18] Maleej, K.; Kelouwani, S.; Dube, Y. and Agbossou, K. Event-Based Electric Vehicle Mass and Grade Estimation. *2014 IEEE Vehicle Power and Propulsion Conference (VPPC)*, **2014**, Coimbra, Portugal, pp. 1-6. doi: 10.1109/VPPC.2014.7007066.

[19] Hong, S.; Lee, C.; Borrelli, F. and Hedrick, J. K. A Novel Approach for Vehicle Inertial Parameter Identification Using a Dual Kalman Filter. *Intelligent Transportation Systems, IEEE Transactions on*, **2015**, vol. 16 (1), pp. 151-161. doi: 10.1109/TITS.2014.2329305.

[20] Jordan, J.; Hirsenkorn, N; Klanner, F. and Kleinsteuber, M. Vehicle Mass Estimation Based on Vehicle Vertical Dynamics Using a Multi-Model Filter. *2014 IEEE 17th International Conference on Intelligent Transportation Systems (ITSC)*, **2014**, Qingdao, China, pp. 2041-2046. doi: 10.1109/ITSC.2014.6958004.

[21] Rhode, S. and Gauterin, F. Online estimation of vehicle driving resistance parameters with recursive least squares and recursive total least squares. *2013 IEEE Intelligent Vehicles Symposium (IV)*, **2013**, Gold Coast, QLD, Australia, pp. 3599-3604. doi: 10.1109/ACC.2012.6314832.

[22] Hong, S.; Smith, T. and Borrelli, F. Vehicle inertial parameter identification using Extended and unscented Kalman Filters.*16th International IEEE Conference on Intelligent Transportation Systems (ITSC 2013)*, **2013**, The Hague, Netherlands, pp. 1436-1441. doi: 10.1109/ITSC.2013.6728432.

[23] Feng, Y.; Xiong, L.; Yu, Z. and Qu, T. Recursive least square vehicle mass estimation based on acceleration partition. *Chinese Journal of Mechanical Engineering*, **2014**, vol. 27 (3), pp. 448458. doi: 10.3901/CJME.2014.03.448.

[24] Bogdanski, K. and Best, M.C. Kalman and particle filtering methods for full vehicle and tyre identification. *Vehicle System Dynamics*, **2018**, vol. 56 (5), pp. 769-790. doi: 10.1080/00423114.2017.1337914.

[25] Zarringhalam, R.; Rezaeian, A. and Melek, W. A comparative study on identification of vehicle inertial parameters. *2012 American Control Conference (ACC)*, **2014**, Montreal, QC, Canada, pp. 3599-3604. doi: 10.1109/ACC.2012.6314832.

[26] Zong, C., Hu, D. and Zheng, H. Dual extended Kalman filter for combined estimation of vehicle state and road friction. *Chinese Journal of Mechanical Engineering*, **2013**, vol. 26, pp. 313. doi: 10.3901/CJME.2013.02.313.

[27] Reina, G., Paiano, M. and Paiano, J.L. Vehicle parameter estimation using a model-based estimator. *Mechanical Systems and Signal Processing*, **2017**, vol. 87, Part B, pp. 227-241. doi: 10.1016/j.ymssp.2016.06.038.

[28] Vargas-Melendez, L; Boada, B.L.; Boada, M.J.L.; Gauchia, A. and Diaz, V., Sensor Fusion Based on an Integrated Neural Network and Probability Density Function (PDF) Dual Kalman Filter for On-Line Estimation of Vehicle Parameters and States, *Sensors*, **2017**, vol. 17 (5), article number 987. doi: 10.3390/s17050987.

[29] Doumiati, M.; Victorino, A.; Charara, A. and Lechner, D. Estimation of road profile for vehicle dynamics motion: Experimental validation, *Proceedings of the 2011 American Control Conference*, **2011**, San Francisco, CA, USA, pp. 5237-5242. doi: 10.1109/ACC.2011.5991595.

[30] Vargas-Melndez, L.; and Boada, B.L.; Boada, M.J.L.; Gaucha, A. and Daz, V. A Sensor Fusion Method Based on an Integrated Neural Network and Kalman Filter for Vehicle Roll Angle Estimation. *Sensors*. **2016**, vol. 16 (9), article number 1400. doi: 10.3390/s16091400.

[31] Boada, B. L., Garcia-Pozuelo, D., Boada, M. J. L. and Diaz, V. A Constrained Dual Kalman Filter Based on pdf Truncation for Estimation of Vehicle Parameters and Road Bank Angle: Analysis and Experimental Validation. *IEEE Transactions on Intelligent Transportation Systems*, **2017**, vol. 18, no. 4, pp. 1006-1016. doi: 10.1109/TITS.2016.2594217.